Palaeogeography, Palaeoclimatology, Palaeoecology 292 (2010) 319–324

Contents lists available at ScienceDirect

Palaeogeography, Palaeoclimatology, Palaeoecology

journal homepage: www.elsevier.com/locate/palaeo

East Asian winter monsoon variability over the last glacial cycle: Insights from a latitudinal sea-surface temperature gradient across the South China Sea

Jun Tian [a,*], Enqing Huang [a], Dorothy K. Pak [b]

[a] State Key Laboratory of Marine Geology, Tongji University, Shanghai 200092, China
[b] Department of Earth Science and Marine Science Institute, University of California, Santa Barbara CA 93106, USA

ARTICLE INFO

Article history:
Received 2 December 2009
Received in revised form 7 April 2010
Accepted 8 April 2010
Available online 14 April 2010

Keywords:
East Asian winter monsoon
South China Sea
Millennial scale
Last glacial/interglacial cycle

ABSTRACT

High-resolution planktonic foraminifer Mg/Ca sea surface temperature (SST) and $\delta^{18}O$ records of IMAGES core MD052896 from the southern South China Sea (SCS) provide a history of East Asian winter monsoon variability over the past 23 kyr. Specifically, we find that the latitudinal SST gradient of the north–south SCS shows promise as a useful proxy of East Asian winter monsoon changes. The ΔSST record of core MD052896 from the southern SCS and ODP site 1145 from the northern SCS documents several positive anomalies indicating East Asia winter monsoon maxima during cold periods of the past 23 kyr, including the H1 and Younger Dryas events. The ΔSST record also indicates that after ~8.5 ka the East Asian winter monsoon strengthened relative to the deglaciation, reaching levels of the last glacial period. Comparison of the SCS ΔSST record with stalagmite $\delta^{18}O$ records suggests that both the East Asian summer and winter monsoons strengthened from the last glacial to the Holocene, and that summer and winter monsoon strength probably are not anti-correlated, at least over the last glacial–interglacial cycle.

1. Introduction

Seasonal reversal of wind directions characterizes the monsoon climate over East Asia and the South China Sea (SCS). Studies of the paleo-monsoon variability provide insights into monsoonal dynamics on millennial, orbital and tectonic time scales, which involves changes in insolation and internal interactions among the atmosphere, oceans, land surfaces and ice sheets (Ding et al., 1994; Wang et al., 2001; Tian et al., 2006; Yancheva et al., 2007a,b,c). Constructing reliable terrestrial or marine proxies is thus a critical aspect of paleo-monsoon studies.

In this respect, terrestrial proxies are better developed than marine proxies because their physical or chemical origins are relatively simple in comparison. The magnetic susceptibility (MS) of loess-paleosol sequences is positively correlated with the production of ultrafine-grained magnetic minerals controlled by summer–monsoon-dominated precipitation-driven pedogenesis in the loess. Presently, dust storm and dust-fall events in China are closely associated with the winter monsoon. The MS and grain size peaks in loess-paleosol sequences are therefore related to strengthened summer and winter monsoons during interglacial and glacial intervals, respectively (Ding et al., 1994; Porter and An, 1995). However, low sedimentation rates and dating difficulties complicate efforts to trace the monsoonal variability on millennial or centennial timescales using loess-paleosol sequences.

Absolutely ^{230}Th dated stalagmite $\delta^{18}O$ records and lake sediment records from South China fill this gap of the paleo-monsoon study on millennial and centennial timescales. Speleothem calcite $\delta^{18}O$ can be interpreted solely in terms of the $\delta^{18}O$ of summer–monsoon-dominated meteoric precipitation and equilibrium fractionation during calcite precipitation (Wang et al., 2001). The precisely dated stalagmite $\delta^{18}O$ records from Dongge, Hulu and Sanbao caves of the South China have recorded the East Asian summer monsoon variability for the past 224 kyr on millennial and centennial timescales (Wang et al., 2008b). The MS, S-ratio, which is a (nonlinear) estimate of the abundance of magnetite compared to that of antiferromagnetic minerals, and Ti content of the Lake Huguang–Maar sediment in South China closely correlate with winter–monsoon-controlled lake redox conditions and aeolian input, and can be used as useful terrestrial proxies of the East Asian winter monsoon (Yancheva et al., 2007a). However, the short lake sediment cores only document a history of winter monsoon variability back to about 16 kyr.

Marine sediments from the marginal seas of the Asian continent exhibit great advantages over terrestrial sediments in this respect, because continuous deep sea sediments with high sedimentation rate extend back to the Oligocene/Miocene boundary in the South China Sea basin (Tian et al., 2008). The difficulty lies in distinguishing monsoonal signatures from those resulting from various other climatic and oceanographic processes, making it difficult to establish marine proxies that give a reliable indication of either winter or summer monsoon strength.

The oceanographic dataset WOA05 (http://www.nodc.noaa.gov/OC5/WOA05/pr_woa05.html) (Locarnini et al., 2006) demonstrates that the annual mean sea surface temperature (SST) gradient between the north and south SCS shows a close relationship with winter monsoon

* Corresponding author.
E-mail address: tianjun@tongji.edu.cn (J. Tian).

0031-0182/$ – see front matter © 2010 Elsevier B.V. All rights reserved.
doi:10.1016/j.palaeo.2010.04.005

strength. Seasonality of SST is significant in the SCS. Summer SST (July, Fig. 1a) is nearly homogenous across the whole SCS, reaching 29 °C, except for the southeastern coast of Vietnam where the SST drops by 1 °C due to coastal upwelling. Winter SST (January, Fig. 1b) is 1–2 °C cooler relative to summer in the southern SCS; whereas a steep temperature gradient develops in the northern SCS during the winter months, with 5–8 °C of cooling relative to summer. The annual mean SST (Fig. 1c) varies from 28 °C to 29 °C in the southern SCS, and from 26 °C to 27 °C in the northern, with a latitudinal SST gradient of 2 °C. We calculated the summer (average of June, July and August), winter (average of December, January and February) and annual mean (average of whole year) SST gradients of two rectangle zones in the northern (19°–20°N, 117°–118°E) and southern SCS (8°–9°N, 111°–112°E) based on the NCEP/NCAR reanalysis database (Fig. 1d). Results show that from the year 1948 to the year 2009 the summer SST gradient changes around 0 °C, and the winter SST gradient varies from 1.3 °C to 3.6 °C. The annual mean SST gradient changes from 0.7 °C to 1.8 °C, accounting for ~50% of the winter SST gradient.

The winter SST in the northern SCS shows a close relationship with the wind direction of the winter monsoon (Fig. 1b). The cold and dry winter monsoon flows southwardly, drastically cooling southeast Asia and the western Pacific Ocean. It also drives the cold water southward along the East China Sea, further reducing the SST in the northern SCS (Fig. 1b). We calculated the monthly mean (January) surface vector wind speed averaged in the rectangle zone (19°–20°N, 117°–118°E) from the northern SCS based on the NCEP reanalysis database (Fig. 1e). Comparison reveals that January vector wind speed is positively related to annual mean SST gradient of the north–south SCS (Fig. 1e). Decadal scale trends indicate that between the years 1948 and 1990, the relatively stable winter monsoon strength corresponded with a relatively stable annual mean SST gradient, whereas between 1991 and 2009, the increased winter monsoon strength corresponded with an expanded annual mean SST gradient. This observation indicates that the latitudinal SST gradient of the north–south SCS is likely a useful proxy of the East Asian paleo-winter–monsoon variability.

Here, we present high-resolution (~200 years) $\delta^{18}O$ and Mg/Ca SST records of the planktonic foraminifer *G. ruber* from IMAGES core MD052896 (08°49.50′N, 111°26.47′E, at 1657 m water depth, Fig. 1) located in the southern SCS. Based on precise AMS ^{14}C dating and comparison with a similar Mg/Ca SST record from ODP Site 1145 (19°35′N, 117°38′E, at 3175 m water depth, Fig. 1) from the northern SCS (Oppo and Sun, 2005), we aim to demonstrate the feasibility of the SST gradient as a useful winter monsoon proxy, and further discuss the East Asian winter monsoon variability over the past 23 kyr. The core MD052896 and the ODP Site 1145 are very close to the center of the south and north rectangle zones respectively, which are chosen for calculating the modern SST gradient of the north–south SCS (see the above introduction).

2. Materials and methods

We took the upper 2 meters of sediment of the core MD052896 and subsampled them at 2 cm interval, equivalent to a time resolution of ~200 years. To be consistent with the SST record from ODP Site 1145 in the northern SCS, we reconstructed the SST record of core MD052896 using the planktonic foraminifer *G. ruber* Mg/Ca (60 specimen, each 0.3–0.36 mm). The Mg/Ca measurements were made at the University of California, Santa Barbara using a Thermo Finnigan Element2 sector inductively coupled plasma mass spectrometer (ICP-MS) following published methods (Lea et al., 2000). We also performed stable isotopic measurements on the planktonic foraminifer *G. ruber* (8 specimen, each 0.3–0.36 mm) in a Finnigan MAT252 mass spectrometer equipped with a Finnigan automatic carbonate device (Kiel III) in State Key Laboratory of Marine Geology, Tongji University. Detailed procedure of these laboratory analyses can be found elsewhere (Tian et al., 2002). The SST reconstruction of ODP Site 1145 (Oppo and Sun, 2005) is based on a

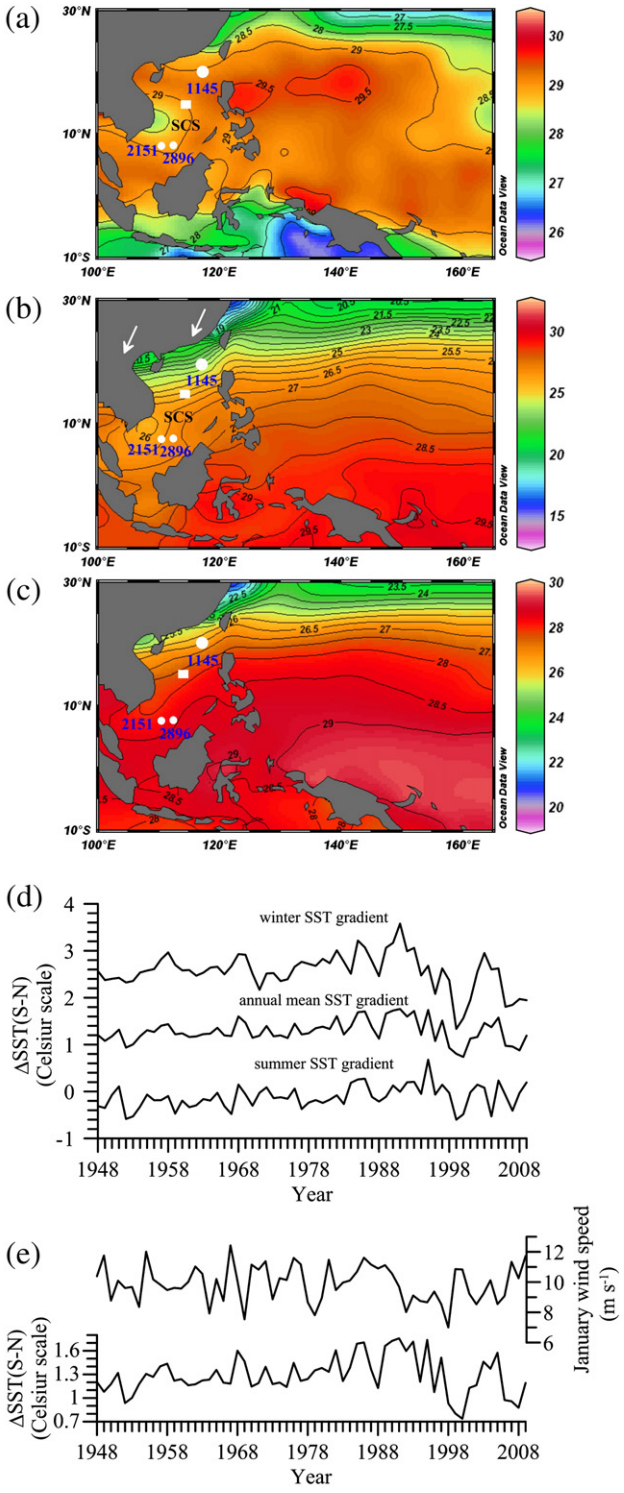

Fig. 1. (a) July SST; (b) January SST; (c) annual mean SST; (d) annual mean, summer and winter ΔSST gradient of the north–south SCS; (e) annual mean ΔSST gradient of the north–south SCS and the January wind speed. Arrows denote the East Asian winter monsoon. Data from a, b, and c comes from WOA05 (http://www.nodc.noaa.gov/OC5/WOA05/pr_woa05.html). Data from d and e comes from NCEP/NCAR reanalysis (http://www.cdc.noaa.gov/cgi-bin/data/timeseries/timeseries1.pl). White squares denote the sediment trap in the middle SCS (Tian et al., 2005). White circles denote studied cores.

depth corrected *G. ruber* equation derived from the Pacific core top calibrations (Dekens et al., 2002). Recently, Huang et al. (2008) developed an in-situ Mg/Ca SST calibration equation based on continuous time series sediment traps at four water depths in the South China Sea, which is similar to that of Dekens et al. (2002). Huang

et al. (2008) found that Mg/Ca is strongly affected by selective partial dissolution in the SCS, even at depths well above the lysocline and calcite saturation depth. Thus, this equation is more suitable for the Mg/Ca based SST reconstruction in the SCS than that from Dekens et al. (2002). We calculate the SST of the core MD052896 and recalculate the SST of the ODP Site 1145 using the *G. ruber* Mg–Ca calibration equation of Huang et al. (2008). The reconstructed average SST for the Holocene is 28.5 °C at the core MD052896 and 26.1 °C at the ODP Site 1145 (Fig. 2b), about 0.5–1 °C cooler than those calculated based on the equation of Dekens et al. (2002) but more consistent with the modern SSTs in the southern and northern SCS respectively. Although other Mg/Ca SST-based records exist from the northern SCS (e.g., Wei et al., 2007) we selected ODP Site 1145 for comparison with our record as they are both based on the planktonic foraminifer species *G. ruber*.

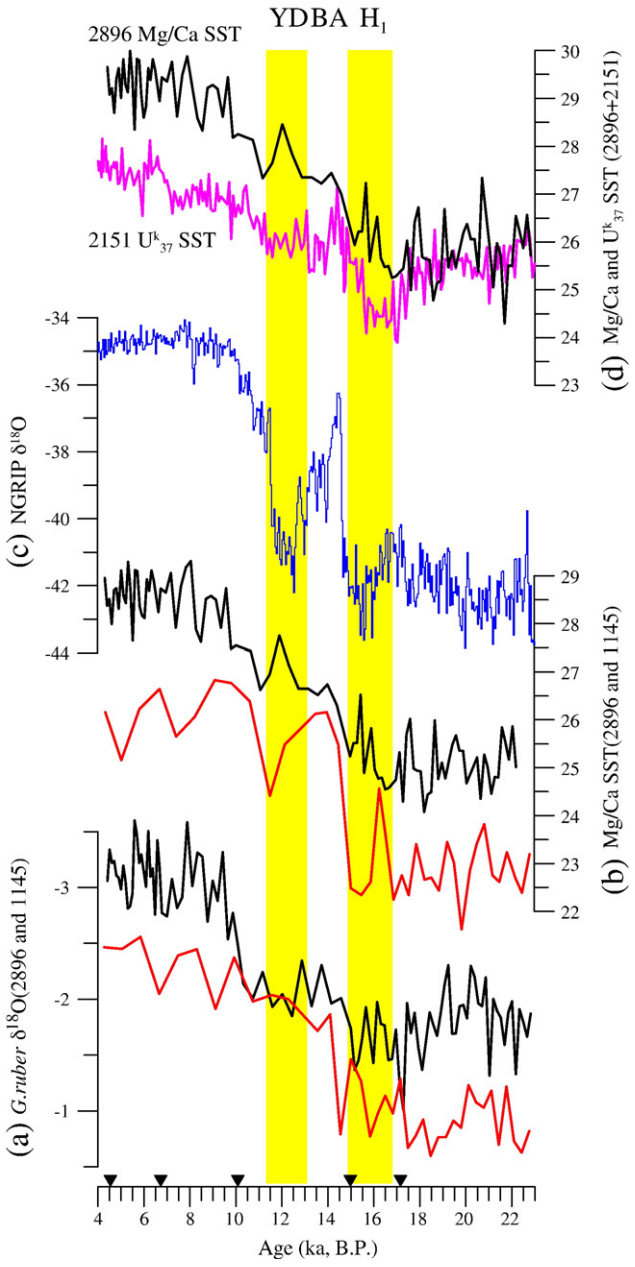

Fig. 2. (a), *G. ruber* δ^{18}O of core MD052896 (black) and site 1145 (red); (b), *G. ruber* Mg/Ca SST of core MD052896 (black) and site 1145 (red); (c), NGRIP δ^{18}O. Black triangles denote AMS ^{14}C dating points from core MD052896; (d), Mg/Ca SST of core MD052896 (black) and U^{K}_{37} SST of core MD972151 (pink). Yellow bars denote the H1 and YD events.

Table 1
Radiocarbon dates and age model of core MD05-2896.

Sample number in laboratory	Depth (cm)	AMS ^{14}C age (year, B.P.)	Errors (year, B.P.)	Calendar age (year)
KIA 32652	6	4420	±130	4604
KIA 32651	50	6315	±50	6778
KIA 32650	82	9465	±60	10,309
KIA 32649	104	13,110	±90	14,999
KIA 32648	130	14,700	±100	17,118

The sediment records were dated by 5 AMS radiocarbon ages on planktonic foraminifers *G. ruber* (1000 individuals, no size limited). AMS ^{14}C dating were performed in Leibniz-Laboratory of Kiel University. ^{14}C ages were converted to calendar ages by using Calib5.01 Program (Stuiver and Reimer, 1993; Stuiver et al., 2005). We adopted a carbon reservoir age of 400 years in the South China Sea although its precise age range is unknown (Stuiver and Braziunas, 1993).

The age model of the records from 0 to 2 m in core MD052896 is based on linear interpolation and extrapolation from five accelerator mass spectrometry (AMS) ^{14}C dates performed in Leibniz-Laboratory of Kiel University, at 6 cm, 50 cm, 82 cm, 104 cm, and 130 cm respectively, which are converted to calendar ages by using Calib5.01 with a carbon reservoir age of 400 years (Table 1). Our discussion of the records is focused on the interpolative time portion constrained among adjacent ^{14}C dates, from 4604 yr to 17,118 yr. Sediment records of ODP Site 1145 extending back to 16 ka are also well constrained by 4 AMS ^{14}C dates. Linear accumulation rates of core MD052896 and ODP Site 1145 in the considered time interval are similar, as high as 10 cm/kyr. The average time resolution of the SST record of Site 1145 is ~500 years for the past 23 ka. In order to compare two SST records with different sample resolutions, we smoothed both records by Gaussian interpolation method at a time step of 500 years, and subtracted the SST of Site 1145 from that of core MD052896 to obtain the ΔSST record, the gradient between the north and south SCS.

3. Results

3.1. Mg/Ca SSTs and G. ruber δ^{18}O in the northern and southern SCS

Both *G. ruber* δ^{18}O and Mg/Ca SST of core MD052896 from the southern South China Sea display a clear glacial transition, although the H1 (Heinrich1) and YD (Younger Dryas) cooling events are not clearly defined (Fig. 2a, b). The Holocene mean SST is ~28.5 °C, nearly 3.3 °C warmer than that of the last glacial (Fig. 2b). The amplitude of the SST fluctuations is ~1.5–2.0 °C during the glacial period but close to and even smaller than 1 °C after the last deglaciation. Prominent increases of the SST at core MD052896 occur between ~16.5 and ~9.5 ka. The initial decrease of *G. ruber* δ^{18}O commences at ~15 ka, lasting for ~1 kyr, then *G. ruber* δ^{18}O remains relatively constant between ~14 and ~10.5 ka. The second decrease of *G. ruber* δ^{18}O commences at ~10.5 ka, and ends at ~9.5 ka.

In the northern SCS, the Mg/Ca SST record of ODP Site 1145 exhibits strong H1 and YD cooling events (Oppo and Sun, 2005), showing 2 °C and 1.5 °C cooling, respectively (Fig. 2b). At ODP Site 1145, both abrupt cooling and rapid warming happen within ~500 yr. Apparently, the general trends of the SST changes in the Holocene are opposite between the southern and northern SCS. While the SST of core MD052896 shows a slight warming trend, that of ODP Site 1145 displays a gradually cooling trend.

3.2. Mg/Ca and $U^{K'}_{37}$ SSTs in the southern SCS

The $U^{K'}_{37}$ index (Pelejero et al., 1999, 2003; Kienast et al., 2001; Zhao et al., 2006) and planktonic foraminiferal Mg/Ca ratios (Oppo and Sun, 2005; Tian et al., 2006; Wei et al., 2007) have been successfully used in reconstructing SST in the SCS. In the SCS, as in many other marine realms, SST reconstructions using different proxies present some disagreement (Jian et al., 2009), and differences are also found

between $U^{K'}_{37}$ and Mg/Ca SSTs. To quantify this discrepancy, we compare the Mg/Ca SST record of core MD052896 with the $U^{K'}_{37}$ SST record of a nearby core MD972151 with similar water depth (8°43.73′ N, 109°52.17′E, at 1597 m water depth, Zhao et al., 2006). Results show that a large discrepancy between the two SST proxies exists during the last glacial cycle (Fig. 2d). Apparently, the $U^{K'}_{37}$ index underestimates SST variations for the last glacial cycle relative to the Mg/Ca SST. The Mg/Ca SST is generally 0.5 °C warmer than that of the $U^{K'}_{37}$ SST before ~16.7 ka, increasing to 1 to 2 °C warmer after ~16.7 ka. The mean Mg/Ca SST is ~28.5 °C for the Holocene, nearly 2 °C warmer than the mean $U^{K'}_{37}$, and is more consistent with the modern annual mean SST in the southern SCS (Fig. 1e).

Previous studies have established several SST timeseries on tectonic (Li et al., 2004), orbital (Jian et al., 2000) and millennial timescales (Wang et al., 1999a) in the SCS for the Pliocene and Pleistocene periods based on different planktonic foraminiferal transfer functions. These SST reconstructions, however, usually show great discrepancies with those derived from alkenone unsaturation and Mg/Ca ratios. As summarized in Jian et al. (2009), for example, the transfer functions usually produce warmer glacials than the Mg/Ca ratio and U^{K}_{37}. The abundances of *Pulleniatina obliquiloculata* and *Neogloboquadrina pachyderma* (dextral) are abnormally high in glacial assemblages in the SCS, which might be the main reason for the biased SST reconstructions by transfer function. Especially in the southern SCS, *P. obliquiloculata* was consistently more abundant during glacials than in the northern SCS (Xu et al., 2005), which can result in a large bias in the SST reconstructions of the northern and southern SCS based on the same transfer function. Steinke et al. (2008) suggests that no-analog behaviour of planktonic foraminifera faunas is responsible for the warm glacial conditions in the SCS as implied by foraminiferal transfer functions and that a more significant surface cooling in the region as implied by terrestrial and geochemical (Mg/Ca ratios; alkenone unsaturation index) marine proxies is a more likely scenario.

4. Discussion

4.1. Interpretation of *G. ruber* Mg/Ca SST gradient

Interpreting *G. ruber* Mg/Ca SST as either seasonal or annual mean SST is important in the interpretation of the SST gradient (ΔSST) of north–south SCS. Modern sediment trap records in the SCS are too short and sparsely distributed to reveal variations in seasonality of planktonic foraminiferal fauna on interannual time scales. For example, the highest *G. ruber* fluxes to the sediment occur during late summer and early autumn in a two-year sediment trap experiment (Lin et al., 2004), but in another three-year sediment trap experiment *G. ruber* dominates the faunal assemblage in winter (Fig. 1, white squares, Tian et al., 2005).

The reconstructed SST records, however, show that *G. ruber* Mg/Ca ratios likely represent the annual mean SST (Fig. 2b). At ODP Site 1145, mean Mg/Ca-derived SST is ~26 °C for the late Holocene (Fig. 2b), much lower than the modern summer mean SST (>29 °C, Fig. 1a) but consistent with the modern annual mean SST at the location of Site 1145 (<27 °C but >26 °C, Fig. 1c). At core MD052896, mean Mg/Ca-derived SST is ~28.5 °C for the late Holocene, resembling the modern annual mean SST (28.5 °C, Fig. 1c) and modern summer mean (29 °C, Fig. 1a) but deviating largely from modern winter mean (26.5 °C, Fig. 1b). Additionally, the average annual mean north–south SCS ΔSST between the years 1948 and 1949 is ~1.3 °C (Fig. 1d), similar to the annual mean ΔSST of 2.2 °C at ~4,0 ka B.P. (Fig. 3a). In the open oceans, planktonic foraminiferal Mg/Ca has been widely used to reconstruct the annual mean SST (Lea et al., 2000; Dekens et al., 2002). Based on the above discussions and the observed close relationship between the winter monsoon strength and the annual mean ΔSST (Fig. 1a), we therefore interpret herein *G. ruber* Mg/Ca-derived ΔSST of the north–south SCS as a proxy of the East Asian winter monsoon.

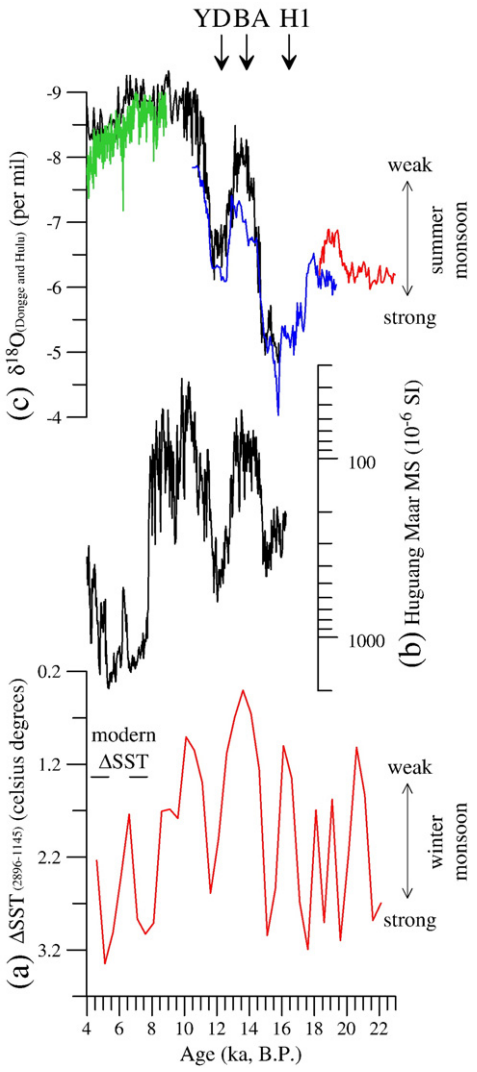

Fig. 3. (a), $\Delta SST_{(2896\text{-}1145)}$; (b), Huguang Maar magnetic susceptibility (Yancheva et al., 2007b); (c), Stalagmite $\delta^{18}O$ of Dongge and Hulu caves (Wang et al., 2001, 2008b). Triangles denote strong East Asian winter monsoon events. Arrows denote YD, BA and H1 events. Dashed line in (a) denotes the modern SST gradient of the north–south SCS which is 1.3 °C.

4.2. East Asian winter monsoon variability during the last glacial cycle

Research on Chinese loess-paleosol sequences (Ding et al., 1994; Porter and An, 1995) reveals that, on orbital timescales, the strength of the East Asian winter monsoon is inversely correlated to the strength of the East Asian summer monsoon, and that the winter monsoon is strong during glacials but weak during interglacials. Conversely, the summer monsoon is strong during interglacials but weak during glacials. This anti-correlated relationship between the East Asian winter and summer monsoon is also apparent on millennial and centennial timescales. Absolutely ^{230}Th dated stalagmite $\delta^{18}O$ records (Wang et al., 2008b) indicate that over the past 224 kyr the summer monsoon was strong during warm interstadials but weak during cold stadials (Wang et al., 2001), while Lake Huguang Maar sediment MS, S-ratio and Ti content records indicate millennial-scale winter monsoon variability that is inversely correlated with the East Asian summer monsoon over the past 16 kyr (Yancheva et al., 2007a). Although the latter result is somewhat controversial (Zhang and Lu, 2007; Zhou et al., 2007), the MS record has proven to be a useful proxy of East Asian winter monsoon variability on millennial timescales (Yancheva et al., 2007b,c).

Our ΔSST record reveals the winter monsoon variability for the past 23 kyr (Fig. 3a). In general, the ΔSST record resembles the Lake Huguang

Maar MS record on both orbital and millennial timescales (Fig. 3a,b). High (low) ΔSST values indicating strong (weak) winter monsoon correspond to high (low) MS values. Even the timing and amplitude of the YD, H1 and BA (Bølling–Allerød) events are identical in the ΔSST and MS records. Large ΔSST occurs in the cold H1 and YD events and in the other cold time intervals (Fig. 3a, blue filled triangles), indicating that on millennial timescales East Asian winter monsoon maxima usually corresponds to cold periods. An inverse correlation between the summer and winter monsoons on millennial timescales can be explained by migrations in the ITCZ (Intertropical Convergence Zone), such that a more northward position of the ITCZ during times of Northern Hemisphere warming would lead to stronger summer monsoon but weaker winter monsoon (Haug et al., 2003; Yancheva et al., 2007a).

Interestingly, comparison between the ΔSST and stalagmite $\delta^{18}O$ records suggests that migration of the ITCZ may not be the only factor controlling East Asian monsoon variability (Fig. 3a, c). As recorded in the ΔSST record (Fig. 3a), the winter monsoon gradually strengthened from the early Holocene, and after ~8.5 ka it became as strong as in the last glacial period (before ~16 ka). Strong winter monsoon conditions after ~8.5 ka are also indicated by higher MS values of the lake Huguang Maar sediment record (Fig. 3b), while the stalagmite $\delta^{18}O$ record (Fig. 3c) indicates that the East Asian summer monsoon has been stronger in the entire Holocene than in the last glacial period. These records indicate that after ~8.5 ka both summer and winter monsoons strengthened relative to the last deglaciation, in contrast to the inversely correlated summer and winter monsoon strengths prior to 16 ka. This suggests that migration of the ITCZ is probably not the unique or dominant factor influencing the East Asian monsoon variations for the last glacial–interglacial cycle.

Wang et al. (1999b) suggested a weaker winter monsoon during the entire Holocene period based on grainsize and clay content records from the northern SCS. However, effects of riverine runoff, which is highly related to the summer monsoon changes, are significant in the northern SCS. Rivers transport a huge amount of terrestrial sediments into the SCS basin, which makes it difficult to distinguish the winter monsoon related composition from the summer monsoon related composition in the deep sea sediments of the SCS based on the method of Parkin and Shackleton (1973).

Support for a strong winter monsoon during the middle Holocene also comes from the diatom concentration record from Lake Huguang Maar. Wang et al. (2008a) demonstrate that the seasonal change in relative abundance of the two dominant diatom taxa, *Aulacoseira* and *Cyclotella*, can be used as a proxy of the strength of the winter monsoon. High *C. stelligera* abundance and high-diatom concentration, which indicate warm conditions and low wind-driven turbulence of the water column, characterize strong summer monsoon conditions, whereas low-diatom concentration and high abundance of *Aulacoseira* species suggests high wind-driven turbulence and therefore strong winter monsoon conditions. The relative concentration records of these two diatom taxa from Lake Huguang Maar indicate that during the early to middle Holocene there were several episodes of intensified winter monsoon conditions comparable to that of the last glacial maximum.

The loess-paleosol record also hints at winter monsoon intensification during the early Holocene. Relatively high dust deposition rates in loess-paleosol profiles from Xifeng, Xunyi and Luochuan also occurred during the early Holocene, indicating a strengthened winter monsoon in east Asia (An, 2000). This is consistent with high lake level records in Australia and Papua New Guinea during the early Holocene (Harrison, 1993). As explained by An (2000), the stronger winter monsoon circulation crossed the equator to strengthen the Australia summer monsoon and may have resulted in increased precipitation, explaining the high lake level in Australia and Papua New Guinea.

Simultaneously intensified East Asian summer and winter monsoons are difficult to explain (An et al., 2001). Our ΔSST record suggests that previous interpretations of an inverse correlation of East Asian summer and winter monsoon strength may not be valid for the entire late Pleistocene. At least from the last glacial to the Holocene, changes in East Asian summer and winter monsoon strength are not anti-correlated, indicating that some important physical mechanisms of the East Asian monsoon variations are still poorly understood.

5. Conclusions

The latitudinal SST gradient of the north–south SCS shows promise as a useful proxy of the East Asian winter monsoon changes. The ΔSST record of core MD052896 and ODP site 1145 documents the millennial scale variability of the East Asia winter monsoon for the past 23 kyr. The positive anomalies of the ΔSST suggest several East Asia winter monsoon maxima during cold stadials for the last glacial–interglacial cycle. We find that after ~8.5 ka the East Asian winter monsoon strengthened relative to the last deglaciation, similar to the strengthening of the East Asian summer monsoon (Wang et al., 2008b). Particularly, the strength of the winter monsoon after ~8.5 ka was as high as during the last glacial period. This suggests that the strength of the East Asian summer and winter monsoons since the last deglaciation are not anti-correlated.

Acknowledgements

We thank all shipboard members on IMAGES cruise MD 147 Leg 1. Funding for this research was provided by the NSFC (Grant No. 40776028, Grant No. 40976024), the NKBRSF (Grant No. 2007CB815902) and the FANEDD (Grant No. 2005036). This research was also sponsored by Shanghai Rising-Star Program (Grant No. 10QH1402600), Fok Ying Tong Education Foundation (111016) and Program for New Century Excellent Talents in University (NCET-08-0401). Jun Tian appreciates the support from Alexander Von Humboldt Foundation on his research in Bremen University. Jun Tian also thank professor Gerold Wefer and Dr. Stefan Mulitza for their kind help on this research.

References

An, Z.S., 2000. The history and variability of the East Asian paleomonsoon climate. Quatern. Sci. Rev. 19, 171–187.
An, Z.S., Kutzbach, J.E., Prell, W.L., Porter, S.C., 2001. Evolution of Asian monsoons and phased uplift of the Himalaya-Tibetan Plateau since Late Miocene times. Nature 411, 62–66.
Dekens, P.S., Lea, D.W., Pak, D.K., Spero, H.J., 2002. Core top calibration of Mg/Ca in tropical foraminifera: refining paleotemperature estimation. Geochem. Geophys. Geosyst. 3, 4. doi:10.1029/2001GC000200.
Ding, Z.L., Yu, Z.W., Rutter, N.W., Liu, T.S., 1994. Towards an orbital time scale for Chinese loess deposits. Quatern. Sci. Rev. 13, 39–70.
Harrison, S.P., 1993. Late Quaternary lake level changes and climates of Australia. Quatern. Sci. Rev. 12, 211–231.
Haug, G.H., Günther, D., Peterson, L.C., Sigman, D.M., Hughen, K.A., Aeschlimann, B., 2003. Climate and the collapse of Maya civilization. Science 299, 1731–1735.
Huang, K.-F., You, C.-F., Lin, H.-L., Shieh, Y.-T., 2008. In situ calibration of Mg/Ca ratio in planktonic foraminiferal shell using time series sediment trap: a case study of intense dissolution artifact in the South China Sea. Geochem. Geophys. Geosyst. 9, Q04016. doi:10.1029/2007GC001660.
Jian, Z., Wang, P., Chen, M.P., Li, B., Zhao, Q., B¨uhring, C., Laj, C., Lin, H.L., Pflaumann, U., Bian, Y., Wang, R., Cheng, X., 2000. Foraminiferal response to major Pleistocene paleographic changes in the southern South China Sea. Paleoceanography 15, 229–243.
Jian, Z., Tian, J., Sun, X., 2009. Upper water structure and paleo-monsoon. In: Wang, P., Li, Q. (Eds.), The South China Sea: Paleoceanography and Sedimentology. Springer Publishing, Berlin, pp. 297–394.
Kienast, M., Steinke, S., Stattegger, K., Calvert, S.E., 2001. Synchronous tropical South China Sea SST change and Greenland warming during deglaciation. Science 291, 2132–2134.
Lea, D.W., Pak, D.K., Spero, H.J., 2000. Climate impact of Late Quaternary equatorial Pacific sea surface temperature variation. Science 289, 1719–1724.
Li, B., Wang, J., Huang, B., Li, Q., Jian, Z., Wang, P., 2004. South China Sea surface water evolution over the last 12 Ma: a south–north comparison from ODP Sites 1143 and 1146. Paleoceanography 19. doi:10.1029/2003PA000906 PA1009.
Lin, H.L., Wang, W.C., Hung, G.W., 2004. Seasonal variation of planktonic foraminiferal isotopic composition from sediment traps in the South China Sea. Mar. Micropaleontol. 53, 447–460.
Locarnini, R.A., Mishonov, A.V., Antonov, J.I., Boyer, T.P., Garcia, H.E., 2006. World Ocean Atlas 2005. In: Levitus, S. (Ed.), Temperature, vol. 1. NOAA Atlas NESDIS 61. U.S. Government Printing Office, Washington, D.C, p. 182.
Oppo, D.W., Sun, Y., 2005. Amplitude and timing of sea-surface temperature change in the northern South China Sea: dynamic link to the East Asian monsoon. Geology 33, 785–788.

Parkin, D.W., Shackleton, N.J., 1973. Trade wind and temperature correlations down a deep-sea core off the Saharan Coast. Nature 245, 455–457.
Pelejero, C., Grimalt, J.O., Heilig, S., Kienast, M., Wang, L., 1999. High resolution $U^{k}37$ temperature reconstructions in the South China Sea over the past 220 kyr. Paleoceanography 14, 224–231.
Pelejero, C., Calvo, E., Logan, G.A., De Deckker, P., 2003. Marine isotopic Stage 5e in the Southwest Pacific: similarities with Antarctica and ENSO inferences. Geophys. Res. Lett. 30. doi:10.1029/2003GL01819.
Porter, S.C., An, Z.S., 1995. Correlation between climate events in the North Atlantic and China during the last glaciation. Nature 375, 305–308.
Steinke, S., Yu, P.S., Kucera, M., Chen, M.T., 2008. No-analog planktonic foraminiferal faunas in the glacial southern South China Sea: implications for the magnitude of glacial cooling in the western Pacific warm pool. Mar. Micropaleontol. 66, 71–90.
Stuiver, M., Braziunas, T.F., 1993. Modelling atmospheric ^{14}C influences and ^{14}C ages of marine samples to 10, 000 BC. Radiocarbon 35, 137–189.
Stuiver, M., Reimer, P.J., 1993. Extended ^{14}C data base and revised CALIB 3.0 ^{14}C age calibration program. Radiocarbon vol. 35, 215–230.
Stuiver, M., Reimer, P.J., Reimer, R.W., 2005. CALIB 5.0 (WWW program and documentation: http://calib.qub.ac.uk/calib/download/).
Tian, J., Wang, P.X., Chen, X.R., Li, Q.Y., 2002. Astronomically tuned Plio-Pleistocene benthic $\delta^{18}O$ records from SouthCh ina Sea and Atlantic–Pacific comparison. Earth Planet. Sci. Lett. 203, 1015–1029.
Tian, J., Wang, P.X., Chen, R.H., Cheng, X.R., 2005. Quaternary upper ocean thermal gradient variations in the South China Sea: implications for east Asian monsoon climate. Paleoceanography 20. doi:10.1029/2004PA001115 PA4007.
Tian, J., Pak, D.K., Wang, P.X., Lea, D., Cheng, X.R., Zhao, Q., 2006. Late Pliocene Monsoon linkage in the tropical South China Sea. Earth Planet. Sci. Lett. 252, 72–81.
Tian, J., Zhao, Q.H., Wang, P.X., Li, Q.Y., Cheng, X.R., 2008. Astronomically modulated Neogene sediment records from the South China Sea. Paleoceanography 23. doi:10.1029/2007PA001552 PA3210.
Wang, L., Sarenthein, M., Erlenkeuser, H., Grimalt, J., Grootes, P., Heilig, S., Ivanova, E., Kienast, M., Pelejero, C., Pflaumann, U., 1999a. East Asian monsoon Climate during the late Pleistocene: high-resolution sediment records from the South China Sea. Mar. Geol. 156, 245–284.
Wang, L., Sarnthein, M., Grootes, P.M., Erlenkeuser, H., 1999b. Millennial reoccurrence of century-scale abrupt events of East Asian monsoon: a possible heat conveyor for the global deglaciation. Paleoceanography 14, 725–731.
Wang, Y.J., Cheng, H., Edwards, R.L., An, Z.S., Wu, J.Y., Shen, C.C., Dorale, J.A., 2001. A high-resolution absolute-dated late Pleistocene monsoon record from Hulu Cave, China. Science 294, 2345–2348.
Wang, L., Lu, H.Y., Liu, J.Q., Gu, Z.Y., Mingram, J., Chu, G.Q., Li, J.J., Rioual, P., Negendank, J., Han, J.T., Liu, T.S., 2008a. Diatom-based inference of variations in the strength of Asian winter monsoon winds between 17,500 and 6000 calendar years. B.P.J. Geophys. Res. 113, D21101. doi:10.1029/2008JD010145.
Wang, Y., Cheng, H., Edwards, R.L., Kong, X.K., Shao, X.H., Chen, S., Wu, J.Y., Jiang, X.Y., Wang, X.F., An, Z.S., 2008b. Millennial- and orbital-scale changes in the east Asian monsoon over the past 224,000 years. Nature 451, 1090–1093.
Wei, G.J., Deng, W.F., Liu, Y., Li, X.H., 2007. High-resolution sea surface temperature records derived from foraminiferal Mg/Ca ratios during the last 260 ka in the northern South China Sea. Palaeogeogr. Palaeoclimatol. Palaeoecol. 250, 126–138.
Xu, J., Wang, P., Huang, B., Li, Q., Jian, Z., 2005. Response of planktonic foraminifera to glacial cycles: Mid-Pleistocene change in the southern South China Sea. Mar. Micropaleontol. 54, 89–105.
Yancheva, G., Nowaczyk, N.R., Mingram, J., Dulski, P., Schettler, G., Negendank, J.F.W., Liu, J.Q., Sigman, D.M., Peterson, L.C., Haug, G.H., 2007a. Influence of the intertropical convergence zone on the East Asian monsoon. Nature 445, 74–77.
Yancheva, G., Nowaczyk, N.R., Mingram, J., Dulski, P., Schettler, G., Negendank, J.F.W., Liu, J.Q., Sigman, D.M., Peterson, L.C., Haug, G.H., 2007b. Replying to: De'er Zhang & Longhua Lu Nature 450. Nature 450, E8–E9.
Yancheva, G., Nowaczyk, N.R., Mingram, J., Dulski, P., Schettler, G., Negendank, J.F.W., Liu, J.Q., Sigman, D.M., Peterson, L.C., Haug, G.H., 2007c. Replying to: H. Zhou et al. Nature 450. Nature 450, E11.
Zhang, D., Lu, L., 2007. Anti-correlation of summer/winter monsoons? Nature 450, E7–E8.
Zhao, M., Huang, C.Y., Wang, C.C., Wei, G.J., 2006. A millennial-scale U^{K}_{37} sea-surface temperature record from the South China Sea (8 N) over the last 150 kyr: Monsoon and sea-level influence. Paleogeogr. Paleoclimatol. Paleoecol. 236, 39–55.
Zhou, H., Guan, H.Z., Chi, B.Q., 2007. Record of winter monsoon strength. Nature 450, E10–E11.